Volume 15
Number 10
14 March 2024
Pages 939-1036

Polymer Chemistry

rsc.li/polymers

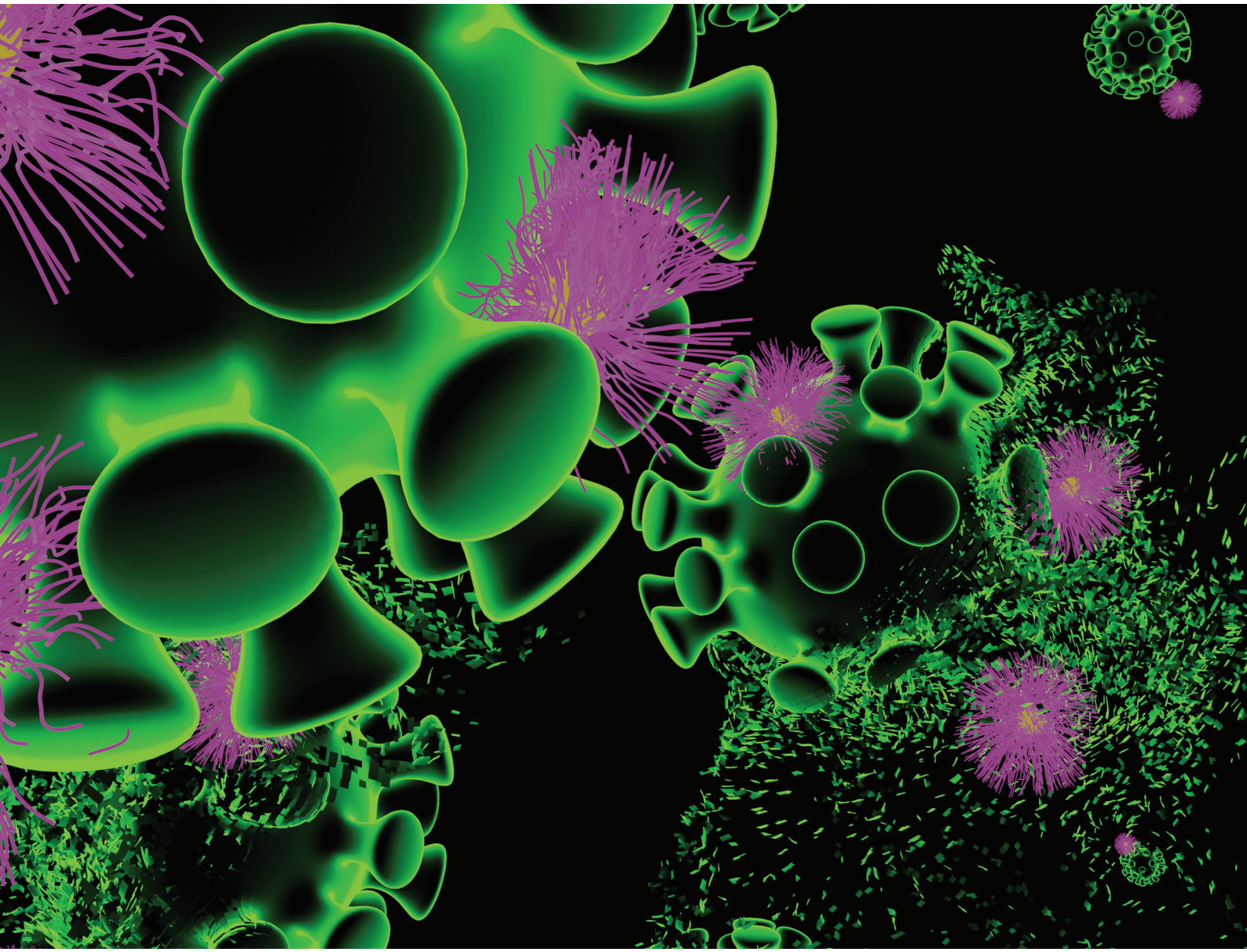

ISSN 1759-9962

ROYAL SOCIETY OF CHEMISTRY

COMMUNICATION
Samuel T. Jones *et al.*
Antiviral mechanism change of poly(styrene sulfonate) through gold nanoparticle coating

Polymer Chemistry

ROYAL SOCIETY OF CHEMISTRY

COMMUNICATION

View Article Online
View Journal | View Issue

Cite this: *Polym. Chem.*, 2024, **15**, 945

Received 31st October 2023,
Accepted 26th January 2024

DOI: 10.1039/d3py01217d

rsc.li/polymers

Antiviral mechanism change of poly(styrene sulfonate) through gold nanoparticle coating†

Lorraine M. Bhebhe, ‡[a] Jungyeon Kim, ‡[a] Luke M. Jones, [a] Elana H. Super [a] and Samuel T. Jones *[a,b]

Viruses are pathogens capable of causing serious global health problems and therefore the development of interventions against them is of paramount importance. One strategy towards designing broad-spectrum antivirals is through the mimicking of sulfonated glycopolymers on the cell surface so that the virion/cell interaction is inhibited by the antiviral material. A number of natural and synthetic polymers have been investigated, however, most show a virustatic mechanism, which is reversible and non-destructive. Herein we present a facile route to virucidal materials by attaching a previously known virustatic polymer, poly(styrene sulfonate), onto gold nanoparticles. We show that it is possible to alter the polymer's mode of action whilst maintaining its low IC_{50} by changing the macromolecular architecture.

Introduction

Viral infections continue to be a significant threat to global health.[1] There are over two hundred viruses currently known to be pathogenic to humans, and up to four new species being discovered every year.[2] In addition, viral outbreaks tend to occur without warning and therefore a rapid, as well as broad-spectrum, response is desired to overcome the barriers associated with other treatments, such as virus specificity or laborious development processes.

A key characteristic of current broad-spectrum antivirals is their extracellular mode of action.[3] One of the ways in which this can be achieved is through the mimicking of cell surface receptors, such as heparan sulfate proteoglycans (HSPGs),[4] or silaic acids.[5] Many viruses, through their viral attachment ligands (VALs), use HSPGs as initial attachment sites.[6] Their role in viral attachment and cell entry for a wide range of viral families is well studied,[4,7–16] including for viruses such as: herpes,[8] papillomaviruses,[9,11] SARS-CoV-2,[17] and HIV-1.[18]

Both natural and synthetic sulfated/sulfonated materials have been shown to act as HSPG-mimics and bind to viruses; their antiviral properties has been known for many years.[19–24] Consequently, a wide array of materials, such as sulfonated nanoparticles,[22,25,26] both natural (such as sulfonated polysaccharides from seaweed) and synthetic polymers,[27–29] have been demonstrated as being broad-spectrum antivirals.

Whilst these materials have displayed broad-spectrum antiviral activity towards HSPG-binding viruses, their application as *in vivo* antivirals remains a challenge. The interaction of these materials has been shown to be reversible and prone to detachment from a virion upon dilution, rending the virus active again; this has been termed as being virustatic.[30–32]

Recently, Groß and co-workers demonstrated the use of poly(styrene sulfonate) (PSS) decorated gold nanoparticles (AuNP) that showed broad-spectrum antiviral activity against a range of enveloped viruses, such as: SARS-COV-2, Zika, respiratory syncytial virus (RSV) and HIV-1.[26] They showed that over a broad range of PSS molecular weights, the nanoparticles showed: broad-spectrum antiviral activity, biocompatibility, and that the antiviral activity was not dependent on the size of the AuNP core itself but rather the size of the polymer. However, they reported that all of the PSS coated AuNPs they studied were virustatic.[26]

An alternative extracellular antiviral approach, termed virucidal, is one where interaction with the material results in an irreversible conformational change in the virion, which permanently prevents viral entry (*e.g.* bleach). This is regarded as the more favourable mode of action, as the virus is destroyed on contact, but it is often associated with greater cytotoxicity limiting its *in vivo* application. However, there have been reports, more recently, of materials with broad-spectrum virucidal properties with low cytoxicity including cycoldextrin,[25] cucurbit[*n*]urils,[22] dendrimers,[28] and nanoparticles.[30]

[a]*Department of Materials and Henry Royce Institute, University of Manchester, Manchester, UK, M13 9PL*
[b]*School of Chemistry, University of Birmingham, Edgbaston, B15 2TT, UK. E-mail: s.t.jones.1@bham.ac.uk*

†Electronic supplementary information (ESI) available: ^{1}H NMR of **L-PSS**, UV/vis spectrum of **PSS-AuNP**, DLS data for PSS-AuNP. See DOI: **https://doi.org/10.1039/d3py01217d**

‡Authors contributed equally to this work.

Here, we report the synthesis of a HSPG-mimicking polymer and its use to functionalise AuNPs to form a virucidal material. Aqueous reversible addition–fragmentation chain transfer (RAFT) polymerisation was used to polymerise sulfonate bearing monomers, which was then used *in situ* during nanoparticle synthesis to generate polymer coated AuNPs. The antiviral activity of the bound and unbound polymer was compared, showing differing antiviral mechanisms, with the gold nanoparticle bound polymer showing an unexpected but desired virucidal mode of action.

Results and discussion

Synthesis of L-PSS and PSS-AuNP

Linear poly(styrene sulfonate) (**L-PSS**) was synthesised *via* aqueous RAFT polymerisation of the monomer sodium 4-vinylbenzenesulfonate with relatively narrow dispersity (Scheme 1, **L-PSS**, $M_{n,Theo}$ = 9500 Da, $M_{n,SEC}$ = 10 800 Da, $Đ$ = 1.1). **L-PSS** in the presence of hydrazine resulted in the cleavage of the thiocarbonylthio bond leading to a thiol terminated PSS (**L-PSS-SH**); comparison of size exclusion chromatography (SEC) traces between cleaved and uncleaved PSS showed no major change in distribution or dispersity (Fig. 1A, **L-PSS-SH**, $M_{n,Theo}$ = 9200 Da, $M_{n,SEC}$ = 10 800 Da, $Đ$ = 1.1). **L-PSS-SH** was then used as the ligand in a modified Brust-Schriffin method, resulting in PSS decorated gold nanoparticles, **PSS-AuNP**. A Brust-Shriffin approach was used in order to give the maximum number of PSS polymers per nanoparticle without a specific size nanoparticle core being selected.

Confirmation of PSS attachment onto the gold core was achieved by thermal analysis and zeta potential measurements. Thermogravimetric analysis (TGA) showed a 31% decrease in total mass between 200 °C and 600 °C, which can be associated with the degradation of the polymer. Dynamic light scattering (DLS) and zeta potential measurements showed that **PSS-AuNP** had a surface charge of −52.6 mV and a hydrodynamic diameter of 140 nm (Fig. S2†). However, upon analysis of **PSS-AuNP** by transmission electron microscopy (TEM), it showed a much smaller average diameter of 3.1 nm with some aggregation being observed on the TEM micrograph (Fig. 1B). This would indicate that there is aggregation of **PSS-AuNP** occurring in solution, leading to a higher than expected particle size observed on the DLS. This is not unexpected when using a Brust-Schriffin approach and samples were used as prepared without any selection of specific sized nanoparticles. The most active nanoparticles by size could be explored further in future work following separation of specific fractions.

Metabolic activity check

MTS assays on hepatocarcinma (HepG2) cell lines, with both **L-PSS** and **PSS-AuNP**, showed no observable difference in HepG2 cell metabolic activity. Since the MTS assay relies on measuring the UV absorbance at λ = 490 nm and AuNPs are also known to have a UV absorbance at this range (Fig. S3†),[33] a control experiment was carried out to measure the UV absorbance of the gold nanoparticles at λ = 490 nm at concentrations of 0–800 μg mL^{-1}. All showed a small amount of UV absorbance in the absence of cells but there was no significant difference between the concentrations (Fig. S4†). Nevertheless, the contribution from the **PSS-AuNP** was subtracted from the UV absorbance values when calculating the cell viability. The metabolic activity of HepG2 when incubated with **L-PSS** and **PSS-AuNP** showed that even 500 μg mL^{-1}, which was the highest concentration of **PSS-AuNP** used in assays, there was no significant difference in the metabolic activity compared with the untreated cells, showing promising potential for *in vivo* use (Fig. 2A).

Antiviral activity of L-PSS and PSS-AuNP

The antiviral activity of **L-PSS** and **PSS-AuNP** was determined using a dose response plaque assay on the HSPG binding virus

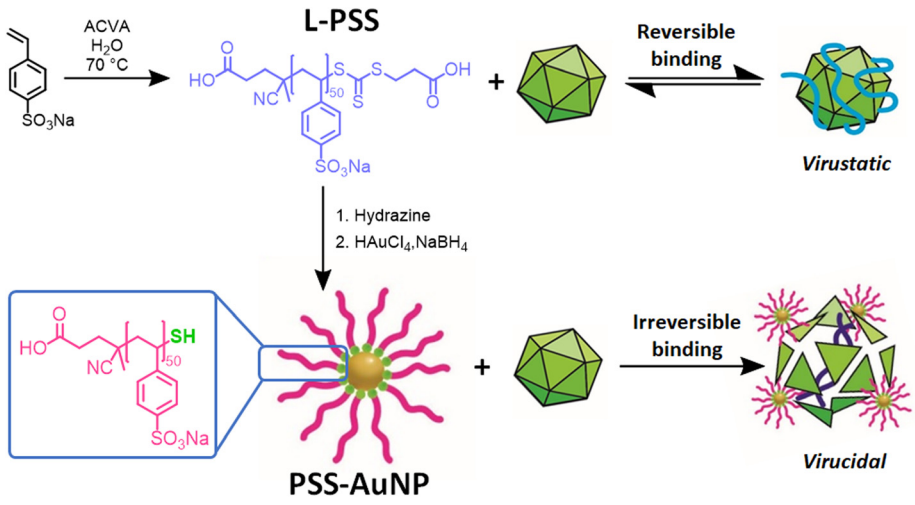

Scheme 1 Synthesis of **L-PSS** and **PSS-AuNP** with the proposed difference in their antiviral mode of action.

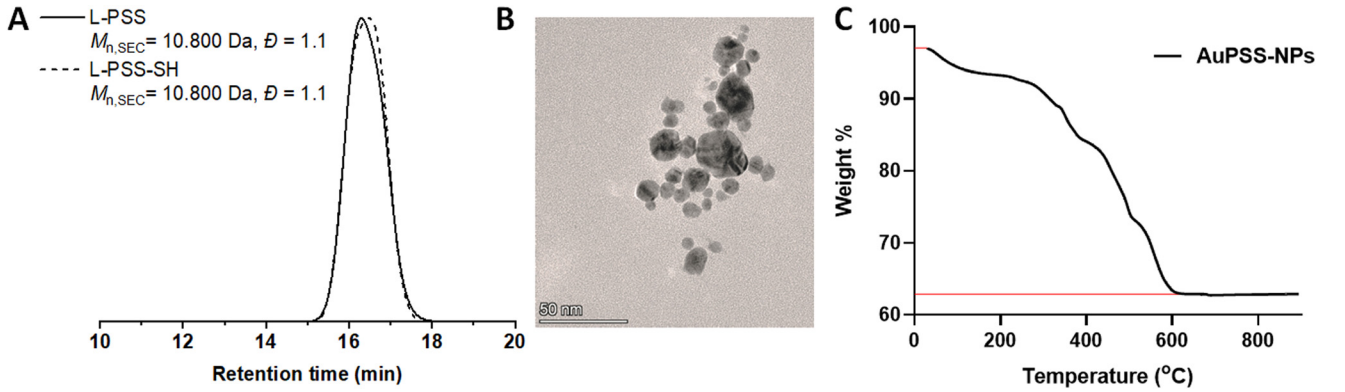

Fig. 1 (A) Normalised SEC traces of **L-PSS** and **L-PSS-SH** measured in aqueous eluent (pH = 9 water : MeOH 70 : 30), (B) TEM image of **PSS-AuNP** (scale bar = 50 nm), and (C) TGA of **PSS-AuNP** showing a mass loss of 31%.

herpes simplex virus-2 (HSV-2), which has been used in previous studies to determine antiviral activity of polymeric and sulfonated materials.[25,30,34]

The IC_{50} values for **PSS-AuNPs** and **L-PSS** on HSV-2 were shown to be IC_{50} = 89.91 ng mL^{-1} and IC_{50} = 27.90 ng mL^{-1}, respectively (Fig. 2B); both of which is significantly (ten-fold) lower than previously reported virucidal materials,[25,34] as well as the previously reported virustatic PSS-coated AuNPs.[26] This highlights the advantages of utilising inherently multivalent polymers during the formation of a nanoparticle core for producing antiviral materials. A weight adjusted IC_{50} was also calculated by using the loss in polymer mass, as calculated from the TGA data; this showed that the IC_{50} value for **PSS-AuNPs**, not including the weight of the gold core, was IC_{50} = 28.02 ng mL^{-1} (Fig. 2C). This shows that the antiviral efficacy of the PSS attached to the gold core had not been altered and remains a potent extracellular antiviral. In addition, fluorescence microscopy imaging confirmed that addition of antiviral to HSV-2, in a 1 : 1 volume ratio, showed a decrease in infection when compared to the no treatment control (Fig. S6†).

In order to show that attachment to AuNPs does not alter the broad-spectrum efficacy of PSS, we used a median tissue culture infectious dose ($TCID_{50}$) assay against respiratory syncytial virus (RSV), which is a single stranded RNA virus with distinct differences to HSV-2, yet is well known to use HSPG during its infection cycle.[35] This confirmed that **PSS-AuNPs** were antiviral against RSV further supporting a potential broad-spectrum application of the material (Fig. S5†).

Antiviral mode of action check through serial dilution

Previous studies on PSS-coated AuNPs have reported a virustatic mode of action,[26] in order to determine the mode of action of **PSS-AuNP** a viral plaque reduction assay was performed.

Here the viral plaque count was monitored over a serial dilution of both **PSS-AuNP** and **L-PSS**; an assay used previously to determine virucidal activity.[25,34,36] Briefly, the antiviral is incubated with virus after which the mixture is incubated onto a cell line followed by serial dilution and the antiviral activity is measured by counting the number of viral plaques formed. In general, if there is a reduction in the number of viral plaques, even with dilution (greater than 99% reduction, or 2log reduction as indicated by the red line in Fig. 3), the mode of action is considered virucidal, since the antiviral activity of the material remains intact over multiple dilutions.

Both **L-PSS** and **PSS-AuNP** were incubated with HSV-2 after which the mixture was diluted up to six-fold and incubated on a Vero cell line. Comparison of the plaque forming units (PFUs) of **L-PSS** and **PSS-AuNP** against the no treatment control (NTC), there was a greater reduction in PFU for **PSS-AuNP** than for **L-PSS**. Plotting the PFUs on a logarithmic scale showed that for **PSS-AuNP** the number of PFUs decreased by over 99% (equivalent to a greater than 2log reduction in PFU) whereas for **L-PSS**, the PFU decrease was only 66% (Fig. 3). These results would indicate that the bound PSS has a virucidal mode of action whereas the unbound PSS has a virustatic mode of action.

Further confirmation of change in mode of antiviral activity, for example by a DNA exposure assay, was performed but with inconclusive results as the highly anionic nature of the polymer interfered with the key component of the assay, DNAse (Fig. S7†).

In conclusion, we demonstrate the switching of antiviral activity of PSS from virusatic to virucidal by changing the conformation of the polymer in solution through coating onto AuNPs. Linear PSS was synthesised by aqeuous RAFT polymerisation and cleaved to the thiol, which was then used as a ligand for an *in situ* gold nanoparticles formation *via* a modified Brust-Schriffin approach. Viral plaque assays with HSV-2 showed that whilst the linear polymer on its own showed virustatic activity, the PSS coated gold nanoparticles showed virucidal activity, indicating that the antiviral mode of action could be altered through PSS architecture with an IC_{50} value that was 10-fold lower than previously reported materials of similar composition. Previous PSS-coated AuNPs have shown significant potential as broad-spectrum antivirals for use *in vivo*, yet their mode of action limits their scope. Here, by accessing a virucidal mode of action, while maintaining low toxicity and

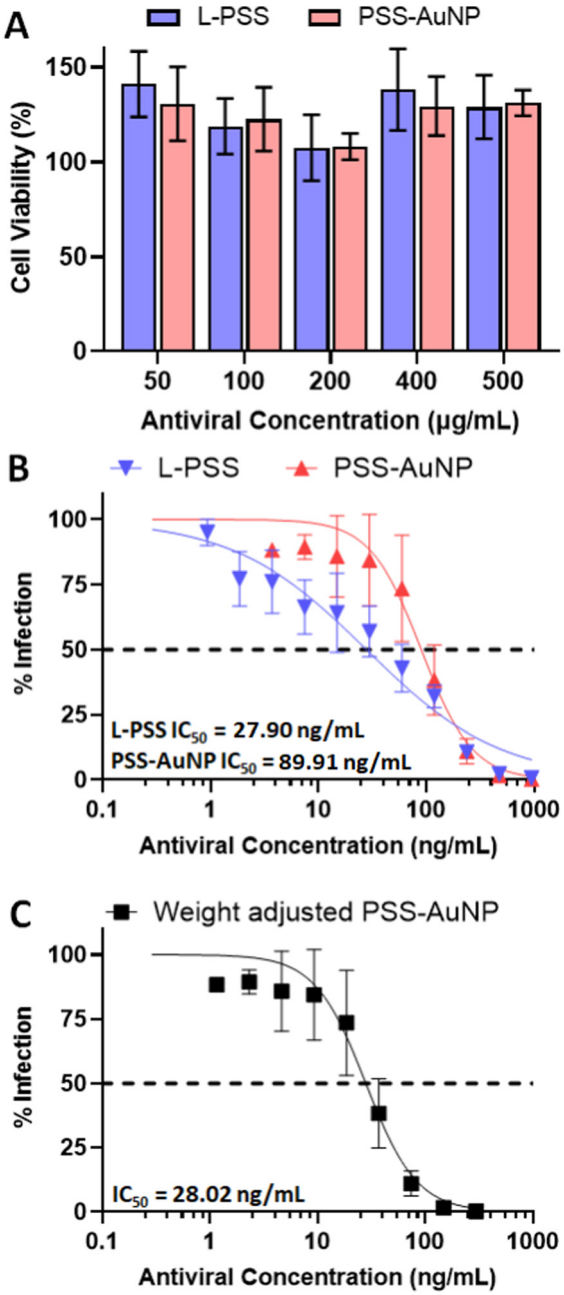

Fig. 2 (A) Metabolic activity of vero cells incubated with **PSS-AuNP** and **L-PSS** (B) dose response curves of **L-PSS** and **PSS-AuNP** against HSV-2 (C) AuNP weight adjusted dose response curve of **PSS-AuNP**.

broad-spectrum efficacy, these materials have significant potential as broad-spectrum *in vivo* virucides.

Materials and methods

Materials

4-((((2-Carboxy-ethyl)thiol)-carbono-thioyl)thio)-4-cyano-pentanoic acid (CTA) was purchased from Boron Pharmaceuticals. Sodium 4-vinylbenzenesulfonate (NaSS), 4,4′-azobis(4-cyanovaleric acid) (ACVA), sodium borohydride ($NaBH_4$), hydrazine solution, MEM Non-Essential Amino Acids were purchased from Sigma-Aldrich. 1 kDa and 10 kDa MWCO RC dialysis tubing were purchased from Spectrum. High glucose Dulbecco's Modified Eagle Medium (DMEM) media, Minimum Essential Medium (MEM), Fetal Bovine Serum (FBS), and L-glutamine, 99% were purchased from ThermoFisher Scientific. CellTiter 96Â® AQueous MTS Reagent was purchased from Promega.

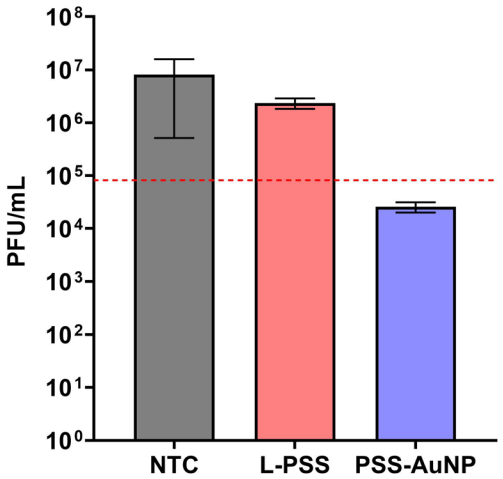

Fig. 3 Viral titer reduction of **L-PSS** and **PSS-AuNP** compared to a no treatment control (NTC) against HSV-2 where the red dotted line indicates a 2log reduction, or greater than 99% reduction, compared to the NTC.

The cell line used in viral culture was Vero (African green monkey fibroblast kidney cells, ATCC CCL-81) kindly donated by Professors Pamela Vallely and Paul Klapper in the University of Manchester Faculty of Biology, Medicine and Health (UoM, FBMH). The cell line used in cytotoxicity studies was HepG2 (a human liver hepatocellular carcinoma cell line, HB-8065) donated by the UoM Biomaterials research group.

Isolates of respiratory syncytial virus (RSV) and herpes simplex virus (HSV-2) were provided by Professors Pamela Vallely and Paul Klapper (University of Manchester, UK), and propagated in vero cells, generating stocks of known log ($TCID_{50}$) per mL.

Cell culture

Vero cells were cultured in high glucose DMEM media supplemented with 2% FBS and 1% L-glutamine. HepG2 cells were cultured in MEME media supplemented with 10% FBS, 1% L-glutamine and 0.1% non-essential amino acids.

Instrumentation

Dynamic light scattering (DLS). DLS and zeta potential measurements were performed using a Malvern Zetasizer Nano equipped with a He–Ne solid-state laser operating at 633 nm and back-scattered light at a scattering angle of 173° at a concentration of 2 mg mL^{-1}.

Thermogravimetric analysis (TGA). TGA was performed using a TGA Q500 under a nitrogen flow of 25 mL min^{--1} from 25 °C to 900 °C at a rate of 10 °C min^{-1}. The sample (31.5 mg) was prepared on an aluminium pan.

Gel permeation chromatography (GPC). PSS was analysed with PSS SEC instrument equipped with a differential refractive index (DRI). The system was equitted with 2X PL aquagel-OH MIXED-M (400 × 7.5 mm) and a PL aquagel-OH guard column. The eluent is 70% Water (pH = 9), 0.2 M $NaNO_3$: MeOH 30% Narrow poly(ethylene oxide) standards were used for calibration between 100–1 300 0000 g mol^{-1}. All samples were filtered through a 0.2 μm nylon filters before injection.

Transmission electron microscopy (TEM). TEM images were recorded using a Thermo Fisher Scientific Talos F200A AEM instrument operating at an accelerating voltage of 200 kV. Samples were prepared by depositing 3 μL of diluted **PSS-AuNPs** onto 400 mesh carbon-coated copper grids for 30 min and then carefully blotted with filter paper to remove excess solution. Mean nanoparticle diameters were determined by ImageJ software.

Experimental

RAFT polymerisation of linear poly(sty-rene sulfonate), L-PSS

NaSS (2.00 g, 9.70 mmol), CTA (59.6 mg, 0.194 mmol), and ACVA (5.44 mg, 0.019 mmol) were dissolved in deionise water and degassed with N_2. The mixture was then left to stir in a oil bath set to 70 °C for 2.5 hours. The reaction was then quenched in an ice bath and dialysed against water.

RAFT agent cleavage to thiol

L-PSS (725 mg, 0.079 mmol) was dissolved in water (2 mL) and hydrazine was added (19.8 mg, 0.396 mmol) and left to stir for 3 hours upon which the colour of the solution changed from clear yellow to colourless. The cleaved **L-PSS** was dialysed against water in 1 kDa MWCO RC dialysis tubing for 3 days.

PSS-AuNP formation

PSS-AuNPs were synthesised using a modified Brust-Schriffin method.[37] Briefly, a 1 mM solution of $HAuCl_4$ was added to a stirring solution of **L-PSS** (9 mM) $NaBH_4$ (1.24 mL of 1 mg mL^{-1} solution) was then added and left to stir for 1 hour, upon which the solution changed colour from pale yellow to amber. The solution was then dialysed against water in 10 kDa MWCO RC dialysis tubing for 3 days to remove any unreacted **L-PSS**.

MTS assays

HepG2 cells were incubated with **L-PSS** and **PSS-AuNPs** at concentrations of 500 mg/mL–50 mg mL^{-1} for 24 hours (37 °C, 5% CO_2). The cells were then washed with PBS and fresh MEME media was added. 20 μL of MTS reagent was added and incubated with the cells for four hours, as per the manufacturer's instructions, and the absorbance at λ = 490 nm was recorded using a plate reader. The significance of differences in absorbance values in cells treated with the materials as compared to NTCs was calculated using the unpaired *t*-test.

HSV-2 dose response assays

A 1 : 100 dilutions of HSV-2 virus stock was treated with a range of concentrations of **L-PSS** and **PSS-AuNPs** for 1 hour (37 °C, 5% CO_2). These samples were then incubated with vero cells (24-well plate of >99% confluency) and incubated for a further hour. The samples were then removed and the cells overlayed with a 3 : 7 ratio of methylcellulose (1.5 wt% methylcellulose in DI) and 2% FBS DMEM overlay (MTC overlay) and incubated for 24–27 h (37 °C, 5% CO_2). After incubation the cells were fixed and stained with crystal violet. Plaque-counting was performed using a standard light microscope.

RSV $TCID_{50}$ assay

The virus stock samples were treated with a concentration range of **L-PSS** and **PSS-AuNPs** for 1 hour (37 °C, CO_2). The samples were then serial diluted across 96 well plates which had been seeded with 6000 vero cells per well the previous day. The plates were incubated for 5 days and then fixed and stained with crystal violet. RSV infectivity across each plate was measured using the Spearman-Karber formula and compared back to NTC plates.

HSV-2 virucidal assay

An inhibitory concentration achieving IC90–IC99 within the virucidal assay was identified for both **L-PSS** and **PSS-AuNPs**. Virus stocks were treated with these concentrations for 1 hour (37 °C, 5% CO_2). The viral samples were then serial diluted across 96 well plates of confluent vero cells (monolayer) resulting in a post-treatment dilution range of 1 : 30–1 : 2.187 × 10^2. The plates were incubated for 1 hour (37 °C, 5% CO_2) before the diluted samples were removed from the plate and replaced with MTC overlay. The plates were then further incubated for 24 hours then fixed and stained with crystal violet. Plaque-counting was performed using a standard light microscope and the pfu mL^{-1} of the viral samples treated with **L-PSS** and **PSS-AuNPs** was calculated and compared to the NTC. As previously described, a difference of 2log or greater was necessary to confirm either material as virucidal, otherwise the material was considered virustatic.[25,30]

Author contributions

L. B. performed all the experiments and wrote the original draft, J. K. wrote the final manuscript, L. M. J. performed the microscopy and contributed in the original manuscript draft, E. S. performed additional assays and contributed in the original manuscript draft, and S. T. J. was involved in conceptualisation, writing of manuscript, and project supervision.

Conflicts of interest

There are no conflicts to declare.

Acknowledgements

L. M. J. acknowledges support from Innovate UK (IUK Project Reference 82583) This work was also supported by the Henry Royce Institute for Advanced Materials, funded through EPSRC grants EP/R00661X/1, EP/S019367/1, EP/P025021/1 and EP/P025498/1. With thanks to Lauren J. Batt and Ayesha Patel for data collection associated with **PSS-AuNP** UV-vis data.

References

1 K. K. Holmes, S. Bertozzi, B. R. Bloom, P. Jha, H. Gelband, L. M. DeMaria and S. Horton, *Major Infectious Diseases*, The International Bank for Reconstruction and Development/The World Bank, 2017.
2 M. Woolhouse, F. Scott, Z. Hudson, R. Howey and M. Chase-Topping, *Philos. Trans. R. Soc., B*, 2012, **367**, 2864–2871.
3 A. Kuroki, J. Tay, G. H. Lee and Y. Y. Yang, *Adv. Healthcare Mater.*, 2021, **10**, 2101113.
4 D. Spillmann, *Biochimie*, 2001, **83**, 811–817.
5 P. Rota, P. La Rocca, F. Bonfante, M. Pagliari, M. Piccoli, F. Cirillo, A. Ghiroldi, V. Franco, C. Pappone, P. Allevi and L. Anastasia, *ACS Infect. Dis.*, 2023, **9**, 617–630.
6 J. Louten, *Essential Human Virology*, Academic Press, Boston, 2016, pp. 49–70.
7 H. Barth, C. Schäfer, M. I. Adah, F. Zhang, R. J. Linhardt, H. Toyoda, A. Kinoshita-Toyoda, T. Toida, T. H. v. Kuppevelt, E. Depla, F. v. Weizsäcker, H. E. Blum and T. F. Baumert, *J. Biol. Chem.*, 2003, **278**, 41003–41012.
8 E. Trybala, J.-Å. Liljeqvist, B. Svennerholm and T. Bergström, *J. Virol.*, 2000, **74**, 9106–9114.
9 T. Giroglou, L. Florin, F. Schäfer, R. E. Streeck and M. Sapp, *J. Virol.*, 2001, **75**, 1565–1570.
10 A. O'Hearn, M. Wang, H. Cheng, C. M. Lear-Rooney, K. Koning, E. Rumschlag-Booms, E. Varhegyi, G. Olinger and L. Rong, *J. Virol.*, 2015, **89**, 5441–5449.
11 L. Cruz and C. Meyers, *PLoS One*, 2013, **8**, e68379.
12 M. Patel, M. Yanagishita, G. Roderiquez, D. C. Bou-Habib, T. Oravecz, V. C. Hascall and M. A. Norcross, *AIDS Res. Hum. Retroviruses*, 1993, **9**, 167–174.
13 C. Summerford and R. J. Samulski, *J. Virol.*, 1998, **72**, 1438–1445.
14 Y. Chen, T. Maguire, R. E. Hileman, J. R. Fromm, J. D. Esko, R. J. Linhardt and R. M. Marks, *Nat. Med.*, 1997, **3**, 866–871.
15 C.-S. Chung, J.-C. Hsiao, Y.-S. Chang and W. Chang, *J. Virol.*, 1998, **72**, 1577–1585.
16 C. J. Mycroft-West, D. Su, I. Pagani, T. R. Rudd, S. Elli, S. E. Guimond, G. Miller, M. C. Z. Meneghetti, H. B. Nader, Y. Li, Q. M. Nunes, P. Procter, N. Mancini, M. Clementi, N. R. Forsyth, J. E. Turnbull, M. Guerrini, D. G. Fernig, E. Vicenzi, E. A. Yates, M. A. Lima and M. A. Skidmore, *bioRxiv*, 2020, 2020.04.28.066761.
17 C. J. Mycroft-West, D. Su, I. Pagani, T. R. Rudd, S. Elli, N. S. Gandhi, S. E. Guimond, G. J. Miller, M. C. Z. Meneghetti, H. B. Nader, Y. Li, Q. M. Nunes, P. Procter, N. Mancini, M. Clementi, A. Bisio, N. R. Forsyth, V. Ferro, J. E. Turnbull, M. Guerrini, D. G. Fernig, E. Vicenzi, E. A. Yates, M. A. Lima and M. A. Skidmore, *Thromb. Haemostasis*, 2020, **120**, 1700–1715.
18 M. Danial and H. A. Klok, *Macromol. Biosci.*, 2015, **15**, 9–35.
19 A. J. Nahmias and S. Kibrick, *J. Bacteriol.*, 1964, **87**, 1060–1066.
20 S. A. Feldman, R. M. Hendry and J. A. Beeler, *J. Virol.*, 1999, **73**, 6610–6617.
21 S. T. Jones, V. Cagno, M. Janeček, D. Ortiz, N. Gasilova, J. Piret, M. Gasbarri, D. A. Constant, Y. Han, L. Vuković, P. Král, L. Kaiser, S. Huang, S. Constant, K. Kirkegaard, G. Boivin, F. Stellacci and C. Tapparel, *Sci. Adv.*, 2020, **6**.
22 L. M. Jones, E. H. Super, L. J. Batt, M. Gasbarri, F. Coppola, L. M. Bhebhe, B. T. Cheesman, A. M. Howe, P. Král, R. Coulston and S. T. Jones, *ACS Infect. Dis.*, 2022, **8**, 2084–2095.
23 V. Ahmadi, C. Nie, E. Mohammadifar, K. Achazi, S. Wedepohl, Y. Kerkhoff, S. Block, K. Osterrieder and R. Haag, *Chem. Commun.*, 2021, **57**, 11948–11951.
24 V. Pirrone, B. Wigdahl and F. C. Krebs, *Antiviral Res.*, 2011, **90**, 168–182.
25 S. T. Jones, V. Cagno, M. Janeček, D. Ortiz, N. Gasilova, J. Piret, M. Gasbarri, D. A. Constant, Y. Han, L. Vuković, P. Král, L. Kaiser, S. Huang, S. Constant, K. Kirkegaard, G. Boivin, F. Stellacci and C. Tapparel, *Sci. Adv.*, 2020, **6**, eaax9318.
26 R. Groß, L. M. Dias Loiola, L. Issmail, N. Uhlig, V. Eberlein, C. Conzelmann, L. R. Olari, L. Rauch, J. Lawrenz, T. Weil, J. A. Müller, M. B. Cardoso, A. Gilg, O. Larsson, U. Höglund, S. A. Pålsson, A. S. Tvilum, K. B. Løvschall, M. M. Kristensen, A. L. Spetz, F. Hontonnou, M. Galloux, T. Grunwald, A. N. Zelikin and J. Münch, *Adv. Sci.*, 2022, **9**, 2201378.
27 F. Schandock, C. F. Riber, A. Röcker, J. A. Müller, M. Harms, P. Gajda, K. Zuwala, A. H. F. Andersen, K. B. Løvschall, M. Tolstrup, F. Kreppel, J. Münch and A. N. Zelikin, *Adv. Healthcare Mater.*, 2017, **6**, 1700748.
28 E. Mohammadifar, M. Gasbarri, V. Cagno, K. Achazi, C. Tapparel, R. Haag and F. Stellacci, *Biomacromolecules*, 2022, **23**, 983–991.
29 D. E. Bergstrom, X. Lin, T. D. Wood, M. Witvrouw, S. Ikeda, G. Andrei, R. Snoeck, D. Schols and E. De Clercq, *Antiviral Chem. Chemother.*, 2002, **13**, 185–195.
30 V. Cagno, P. Andreozzi, M. D'Alicarnasso, P. J. Silva, M. Mueller, M. Galloux, R. L. Goffic, S. T. Jones, M. Vallino, J. Hodek, J. Weber, S. Sen, E.-R. Janeček, A. Bekdemir, B. Sanavio, C. Martinelli, M. Donalisio, M.-A. R. Welti,

J.-F. Eleouet, Y. Han, L. Kaiser, L. Vukovic, C. Tapparel, P. Král, S. Krol, D. Lembo and F. Stellacci, *Nat. Mater.*, 2018, **17**, 195–203.
31 V. Cagno, C. Tintori, A. Civra, R. Cavalli, M. Tiberi, L. Botta, A. Brai, G. Poli, C. Tapparel, D. Lembo and M. Botta, *PLoS One*, 2018, **13**, e0208333.
32 S. T. Jones, *J. Mater. Sci.*, 2020, 1–4.
33 V. Amendola and M. Meneghetti, *J. Phys. Chem. C*, 2009, **113**, 4277–4285.
34 E. Mohammadifar, M. Gasbarri, V. Cagno, K. Achazi, C. Tapparel, R. Haag and F. Stellacci, *Biomacromolecules*, 2022, **23**, 983–991.
35 V. Cagno, E. D. Tseligka, S. T. Jones and C. Tapparel, *Viruses*, 2019, **11**, 596.
36 B. Shogan, L. Kruse, G. B. Mulamba, A. Hu and D. M. Coen, *J. Virol.*, 2006, **80**, 4740–4747.
37 O. Uzun, Y. Hu, A. Verma, S. Chen, A. Centrone and F. Stellacci, *Chem. Commun.*, 2007, 196–198.